ACS Energy LETTERS

http://pubs.acs.org/journal/aelccp

LETTER

Photovoltage Behavior in Perovskite Solar Cells under Light-Soaking Showing Photoinduced Interfacial Changes

Jiangang Hu,[†,§] Ronen Gottesman,[†,§] Laxman Gouda,[†] Adi Kama,[†] Maayan Priel,[†] Shay Tirosh,[†] Juan Bisquert,[*,‡] and Arie Zaban[*,†]

[†]Department of Chemistry, Center for Nanotechnology & Advanced Materials, Bar-Ilan University, Ramat Gan 52900, Israel
[‡]Institute of Advanced Materials (INAM), Universitat Jaume I, 12006 Castelló, Spain

Supporting Information

ABSTRACT: The photovoltage of perovskite solar cells (PSCs) was studied over a wide range of light intensities, showing changes from pristine to light-soaking (LS) conditions, explained using a specific model of spatial charge distribution. Migration of ions and vacancies under photovoltage conditions results in localized charge redistribution manifested as positive charge accumulation at the TiO_2 or TiO_2–MgO interlayer–perovskite interface, signifying photoinduced interfacial upward band bending. Consequentially, generation of an electrostatic potential (V_{elec}) and an increase in interfacial recombination rate are confirmed. The magnitude and effect of V_{elec} and interfacial recombination on the photovoltage depend on the illumination intensity and on the LS duration. PSCs with mesoporous Al_2O_3 showed similar changes, validating the role of the compact TiO_2. Faster generation and a gradual increase of V_{elec} are apparent under LS, which expresses the constant migration of ions and vacancies toward the interface. The nonrigid TiO_2–perovskite interface calls for a vital perspective change of PSCs.

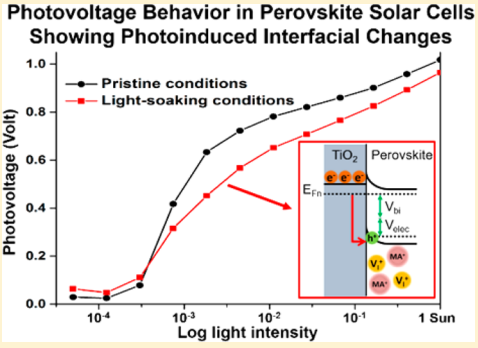

Organometal halide perovskites are regarded as promising light-harvesting materials for low-cost photovoltaics, with solar cell power conversion efficiencies currently exceeding 22%. However, despite their remarkable efficiencies, several issues that are detrimental to perovskite solar cell (PSC) performance are still unresolved.[1] One major concern is fluctuations and changes in device performance under working conditions,[2] which impede further steps toward PSCs' commercialization as cheap and highly efficient devices for optoelectronic applications.[3]

An increasing number of studies suggest that ion migration during the PSCs' operation is responsible for the aforementioned phenomena and that the movement of ions and vacancies can be activated by changing the temperature or by an electrical field.[3−10] It has been shown that at open-circuit voltage conditions, the migration of ions and vacancies results in localized charge redistribution manifested as positive charge accumulating at the electron-selective contact–perovskite interface.[11,12] Consequently, this will lead to formation of an energy barrier hindering charge transfer from the perovskite to the TiO_2[13−15] and buildup of an internal electric field at the interface that is opposite the built-in electric field. Zarazua et al. have suggested light-induced upward band bending at the interface[16] based on accumulation capacitance interpretation under illumination. Hence, when the solar cell is illuminated and set at an open-circuit voltage, significant migration of positive ions and vacancies occurs toward the interface, leading to a drastic modification of the kinetics of the charge transfer processes by changing the conditions at the contact–perovskite interface.

The accumulation of ions and vacancies changes the interface by affecting the concentration and recombination rates of the photogenerated electronic carriers, and thus, the photovoltage is expected to change and to decay depending on the conditions at the interface. To allow for ions and vacancies to accumulate and slowly build up and change the energetics at the interface, the illuminated devices should be under electric field at any one of the following conditions: (i) at open-circuit voltage,[16,17] (ii) at maximum power point,[3] and (iii) during a current–voltage scan with a scan rate that would allow ion accumulation at the interface.[18] Another role of the accumulated ions is to shield and modify the electrical field distribution in the bulk perovskite.[19,20]

Received: March 9, 2017
Accepted: April 5, 2017
Published: April 7, 2017

© 2017 American Chemical Society

DOI: 10.1021/acsenergylett.7b00212
ACS Energy Lett. 2017, 2, 950−956

Recently, we demonstrated a photoinduced interfacial phenomena in $CH_3NH_3PbI_{3-x}Cl_x$ solar cells between the electron-selective contact (TiO_2 or TiO_2–PCBM interlayer) and the perovskite, interpreted from photovoltage decays.[17] By only changing the electron-selective contact and measuring the PSCs under the same conditions, we showed that the photoinduced phenomena originated from the energetic changes at the interface. Clearly, this is a dramatic change in our consideration and treatment of solar cells as this phenomenon also plays an important role in operation conditions and current–voltage scans of the solar cell.

The quantitative model that explained our experimental results[17] is summarized in Figure 1, which displays an energy

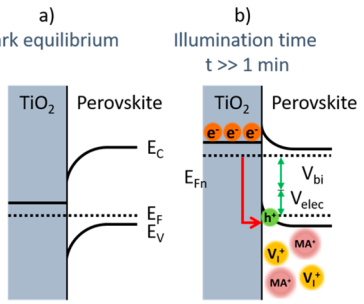

Figure 1. Energy diagram at the TiO_2–perovskite contact in open-circuit conditions at two different stages: (a) under dark without migrating positive cations and vacancies and (b) after a substantial illumination time of $t \gg 1$ min. The red arrow depicts major interfacial recombination. V_{elec} is the electrostatic potential that contributes to the built-in potential, V_{bi}.

diagram of the TiO_2–perovskite interface, which is also the basis of the current study. After a long dark storage period, the state of the system is shown in Figure 1a (the model assumes that band bending inside of TiO_2 and at the anode is negligible). Under illumination, the steady-state distribution will take time to construct. The charging time of the interface can take several minutes, and upon prolonged light-soaking (LS) ($t \gg 1$ min), the distribution of carriers at the interface evolves, causing the hole concentration at the interface to increase due to an overlap between the valence band and the Fermi level of the perovskite; at this point, the system reaches the state seen in Figure 1b. The accumulation of holes causes major interfacial recombination (red arrow), which is in contrast to the minor recombination rate that occurs after a short illumination time, before the substantial accumulation of holes at the interface. Furthermore, the electron Fermi level, E_{Fn}, can still rise further by building the interfacial band bending. This feature creates an additional electrostatic potential, V_{elec}, as a result of the electric field formed across the junction due to the accumulation region. In Figure 1b, the electrostatic potential, V_{elec}, is seen to contribute to the built-in potential, V_{bi}, and increases the overall photovoltage. This electrostatic component is mainly seen when the light is turned off, and it decays very slowly and is understood as the slow reverse migration of ions and vacancies. This demonstrates how the contact–perovskite interface is "nonrigid" as it slowly builds up and changes during illumination and recovers even more slowly. Here, it is considered that a contact containing a pure organic component like PCBM is less rigid that the contact TiO_2/perovskite because the organic layer is able to accommodate surface changes like ionic charge by structural rearrangement.

The dynamic photoinduced interfacial changes make it apparent that the photovoltage will also change with illumination time and intensity. Thus, studying the photovoltage behavior at different illumination intensities under LS is required, in order to gain more insights on the dynamic processes at the contact-perovskite interface.

In this work, we studied the photovoltage decay of $CH_3NH_3PbI_{3-x}Cl_x$ PSCs under LS and its behavior over a wide range of light intensities ($1 \times 10^{-4} < I_0 < 1$ sun). Note: we kept a constant LS intensity $I_0^{LS} = 1$ sun throughout this study to distinguish between it and I_0 effects as photoinduced changes are also dependent on the I_0^{LS} magnitude.[21] We saw an electrostatic potential (V_{elec}) formed in addition to the built-in potential (V_{bi}), which increased the photovoltage at low light intensities, whereas at higher intensities a reduction in photovoltage was observed due to higher interfacial recombination. The magnitude and effect of interfacial recombination on the photovoltage are very much dependent on the illumination intensity that generates V_{bi} and also on the duration of the LS.

In order to validate that the observed photoinduced changes originated at the electron-selective contact–perovskite interface and to examine the role of the mesoporous (mp)-TiO_2, we fabricated three sets of mesoporous PSCs with slightly modified electron-selective contact–perovskite interfaces. In addition to standard PSCs with semiconductive mp-TiO_2,[22] the other two configurations were PSCs with an extremely thin interlayer of MgO deposited on the TiO_2 prior to perovskite deposition (designated mp-TiO_2–MgO, although the compact TiO_2 was also coated with MgO) and PSCs with an insulating mp-Al_2O_3 scaffold on top of compact TiO_2 contacts. We show that the photoinduced changes occur in all three types of PSCs with modified interfaces with only minor changes in lifetime values and decay kinetics. This proves that the origin of the dynamic phenomena is at the electron-selective contact–perovskite interface rather than from the bulk or the interface with the hole-selective contact. Furthermore, this validates that the role of the compact TiO_2 layer is significant in determining the photovoltage in comparison to the mesoporous oxide, as previously reported by us.[23]

All of the measurements were conducted in open-circuit conditions under continuous nitrogen flow, and prior to them, the devices were kept in the dark in a nitrogen environment. It is important to emphasize that the cells were held at open-circuit and measured under dark and light conditions without any bias pretreatments. This is in contrast to performing an *iV* measurement where the voltage is scanned passed the open-circuit and short-circuit points in both the ascending and descending curves, which can lead to a significant current–voltage hysteresis.[24] The illumination source for the wide range of I_0 values and LS was a computer-controlled array of calibrated white LEDs. All LEDs were "cold" light sources, and the PSCs' temperatures were verified by using a thermocouple to be constant during the LS. The measurements of both the open-circuit voltage decay (OCVD) and the photovoltage dependence on I_0 were conducted in three consecutive stages as follows: (i) a reference measurement, taken after an overnight dark storage, (ii) a LS stage, where each measurement was performed after a constant time interval of LS at $I_0^{LS} = 1$ sun, and (iii) a dark recovery stage, where the LS source was turned off and the measurements were performed at time intervals

DOI: 10.1021/acsenergylett.7b00212
ACS Energy Lett. 2017, 2, 950–956

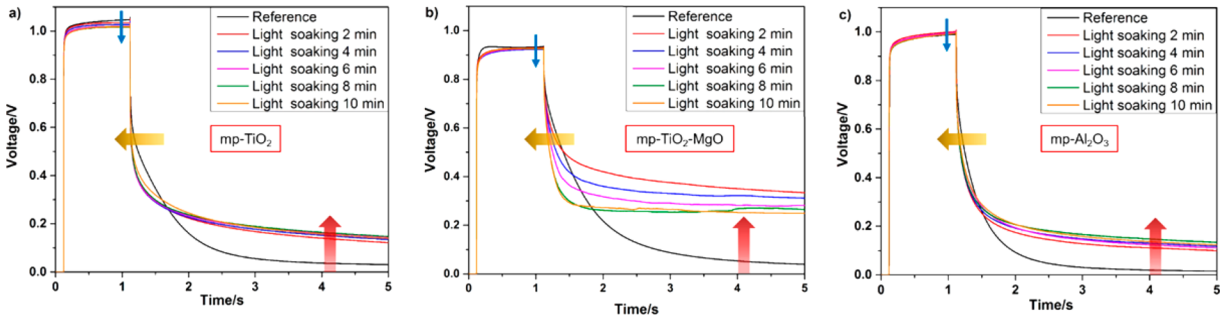

Figure 2. OCVD data of PSCs with three different structures, (a) mp-TiO_2 PSC and (b) mp-TiO_2-MgO PSC, and (c) mp-Al_2O_3, showing the reference and LS stage measurements. The data of the device with a mp-TiO_2 structure (a) are taken from a similar set of measurements published in ref 17, with permission from Elsevier.

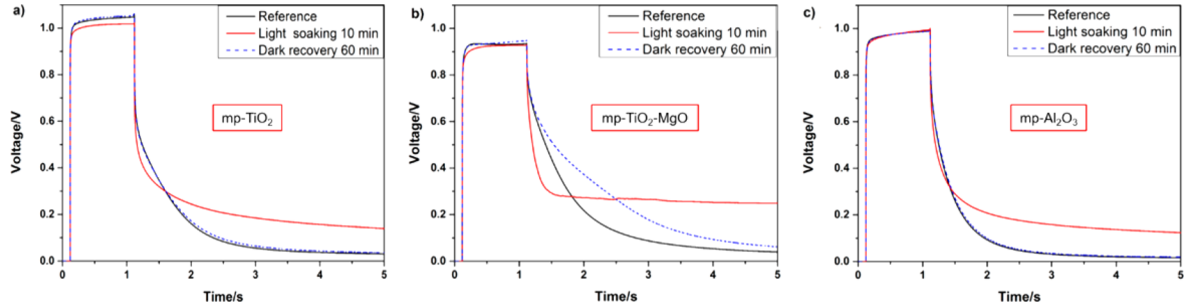

Figure 3. Summarized OCVD plots of the PSCs with three different structures.

identical to the LS time intervals. In the OCVD measurement, the solar cell was held at open-circuit in the dark, and a red LED was turned on for 1 s to generate photovoltage. When the red LED was turned off, the OCVD was recorded. Photovoltage vs log I_0 plots were acquired by measuring the stabilized photovoltage at 12 different light intensities in the range of $1 \times 10^{-4} < I_0 < 1$ sun. In all LS measurement stages, the LS source was turned off right before each measurement. We fabricated, measured, and compared hundreds of PSCs with all three different interfaces as we have an established capability to fabricate multiple PSCs on large-area substrates and perform high-throughput measurements and characterizations.[25,26] Exemplary *iV* curves of the three devices appear in Figure S1. The devices studied here have shown average efficiencies of ~12−15%, depending on the structure, with mp-Al_2O_3 PSCs showing higher hysteresis than the other two structures.

We performed OCVD measurements where the 1 s pulse intensity was $I_0 = 1$ sun and the LS intensity was $I_0^{LS} = 1$ sun (2 min intervals), seen in Figure 2. The electrostatic component decays very slowly in the dark, which makes that OCVD measurements are ideal to observe V_{elec} separately compared to the interfacial recombination. Similar changes in the OCVD were observed in all three PSCs configurations, in both the LS and dark recovery stages (Figures 2 and S2), but slightly to a different extent.

Overall, three kinds of gradual photoinduced changes in the open-circuit voltage are observed: (i) a change in the photovoltage during the 1 s illumination time (marked by the blue arrow), showing evidence of higher interfacial recombination during illumination, which appears to be less severe in the mp-TiO_2−MgO and mp-Al_2O_3 PSCs in comparison to the mp-TiO_2 PSC; (ii) a change in the decay rate (marked by the yellow arrow), which refers to rapid recombination in the interface once the light is turned off, hence the almost immediate drop in voltage; and (iii) buildup of a dark-voltage component, marked by the red arrow. Figure 3 summarize the OCVD measurements of the three different structured PSCs, proving that the electron-selective contact−perovskite interface is the origin of the observed photoinduced changes.

A considerable difference is seen in the magnitude of changes between PSCs with mp-TiO_2−MgO contact and the others. A calculation of the recombination lifetime vs voltage in all three reference measurements showed that the lifetime in mp-TiO_2−MgO PSCs is 1 order of magnitude higher than the lifetimes in the mp-TiO_2 and mp-Al_2O_3 PSCs.[27] However, in the LS measurements, the lifetimes of all three kinds of PSCs decreased (due to increased recombination) to practically identical values and recovered back in the dark recovery stage. Another striking difference was observed in the electrostatic component, V_{elec}. Whereas in the mp-TiO_2 and mp-Al_2O_3 PSCs a long tail of $V_{elec} \approx 150$ mV was seen already after 2 min of illumination, in the mp-TiO_2−MgO PSC, the magnitude of V_{elec} was surprisingly twice as high, ~300−400 mV. We also note that the devices with mp-TiO_2−MgO showed the lowest hysteresis among the three, seen in Figure S1. A detailed study of the origin of these differences is out of the scope of this work. However, we briefly propose two possible explanations (or a combination of both), derived from the modified interface. The first explanation can be passivation of traps by the MgO layer, which can increase the electrons' lifetimes, and the second explanation can be a slightly different band bending/alignment at the interface (more downward in the dark), but under illumination, a similar alignment is attained. This may explain how the modified contact can affect different alignments along the interface of ions, which can lead to different band bending, or other elements that are affected by recombination at lower voltages.

In order to study the dynamic interfacial phenomena dependence on illumination intensity, I_0, we measured the photovoltage behavior as a function of I_0. Figure 4a shows a

DOI: 10.1021/acsenergylett.7b00212
ACS Energy Lett. 2017, 2, 950−956

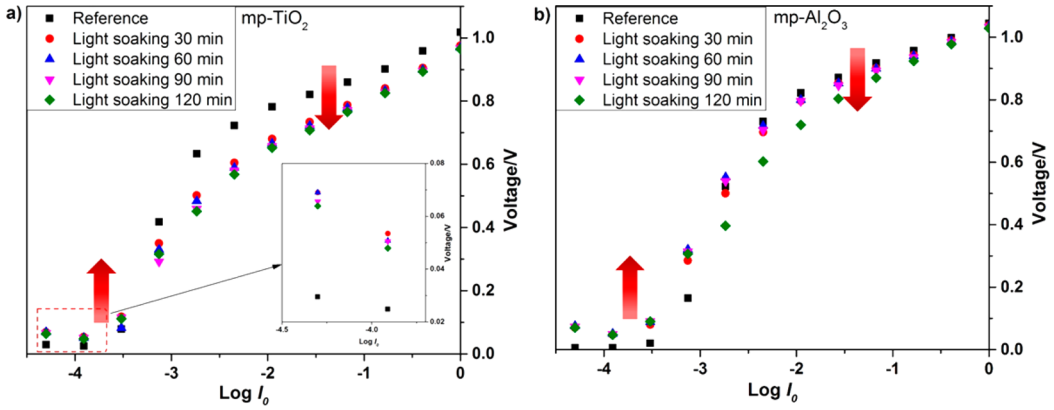

Figure 4. Photovoltage vs log I_0 behavior of PSCs with mp-TiO_2 and Al_2O_3 scaffolds after long dark storage in comparison to prior LS (I_0^{LS} = 1 sun). (a) mp-TiO_2 PSC and (b) mp-Al_2O_3 PSC.

photovoltage vs log I_0 plot of the reference measurement of a mp-TiO_2 PSC in comparison to four consecutive measurements (after LS for 30, 60, 90, and 120 min). Full reversibility to the initial photovoltage values occurred in the dark recovery stage (Figure S3a); however, the recovery was much slower than the changes under illumination, the same as in other reported studies.[17,28] Furthermore, the observed effects were not restricted only to PSCs with mp-TiO_2. Figures 4b and S4b show the photovoltage vs log I_0 behavior for PSCs with a mp-Al_2O_3 scaffold, where smaller changes in the photovoltage and faster recoveries were noticed. We propose that this difference is due to the lower interfacial area of the TiO_2–perovskite, meaning that less interfacial recombination occurs. A similar thing can be claimed in regard to the OCVD data of complementary PSCs, where the interfacial recombination (blue arrow) was higher in mp-TiO_2. Note that the time intervals in the LS stage were 30 min in order to emphasize the photoinduced changes in photovoltage throughout the wide range of I_0. Shorter time intervals gave smaller photoinduced changes, as we also show here in the OCVD measurements.

The observed photoinduced changes can be approximately divided into two light intensity ranges, (i) $1 \times 10^{-4} < I_0 < 1 \times 10^{-3}$ sun, where an increase of ~50 mV in the photovoltage was observed, designated to be V_{elec}, and (ii) $1 \times 10^{-3} < I_0 < 1$ sun, where a decrease of ~50–150 mV (dependent on the I_0 magnitude) in the photovoltage occurred and refers to an increase in the interfacial recombination as I_0 increases. Another important observation seen in Figure 4 is the slope decline at $1 \times 10^{-3} < I_0 < 1$ sun of the measurements performed during the LS stage in comparison to the reference measurement. A slope decline in the photovoltage vs log I_0 plot is an indication of increased recombination, as we have shown in the past.[23,29] A photoinduced slope decline in the mp-Al_2O_3 PSC was also observed; however, the decline was more moderate, presumably due to the lower interfacial area of the compact TiO_2 and the perovskite.

The experimental observations shown here are highly correlated with our model,[17] and we have examined the generation and decay kinetics of V_{elec} to further strengthen it. Figure 5 shows OCVD values (recorded 5 s after the light was turned off) vs the time of the specific measurement in relation to the reference measurement (designated at t = 0 min). Both mp-TiO_2 and mp-Al_2O_3 PSCs were measured where the 1 s light pulses were either $I_0 = 1 \times 10^{-2}$ or 1 sun, designated as low and high I_0, respectively. The data points that appear in the white column were taken during the LS stage, and the data points that appear in the gray, dark recovery area were taken at the dark recovery stage.

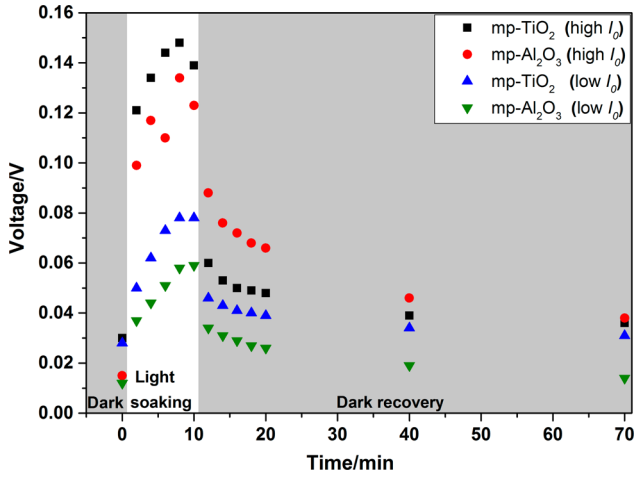

Figure 5. Open-circuit voltage values in the dark from OCVD measurements in all three stages: dark (reference), LS, dark recovery. The 1 s light pulses used to generate the photovoltage were either $I_0 = 1 \times 10^{-2}$ or 1 sun, designated low and high I_0, respectively.

Fast generation of V_{elec} is apparent during the LS stage, and its gradual increase expresses the constant migration of ions and vacancies toward the interface during LS illumination. It is also noticeable that V_{elec} is somewhat dependent on the applied I_0, which means that 1 s of illumination is enough time for the ions to partially rearrange at the interface. When examining V_{elec} in the dark recovery stage, a striking difference in the decay rate appears between the two stages (LS → dark recovery), seen as a bigger drop in voltage when I_0 was high.

To quantify the kinetics of V_{elec}, we calculated the open-circuit voltage change rate during the LS and dark recovery stages (in the mp-TiO_2 PSC). The decay rate of V_{elec} in the LS stage is ~3–4 times higher on average than its decay in the dark recovery stage. This difference can reflect diverse ion migration processes in both stages. Under illumination conditions, ion migration is facilitated by electronic charge screening, while under dark conditions, the overall conductivity decreases. Under I_0^{LS} illumination, V_{bi} between the two contacts generates an electrical field across the perovskite that drives ion drift (V_{elec} buildup), and in the dark, ions diffuse due

DOI: 10.1021/acsenergylett.7b00212
ACS Energy Lett. 2017, 2, 950–956

to a concentration gradient (V_{elec} decay). The fast V_{elec} buildup at the beginning of the LS is attributed to the strong effect of the electrical field. Therefore, the fast migration of iodide and its vacancies induces quick charge accumulation at the interface, which screens V_{bi} and slows down the drift.[30]

In summary, we have studied the photovoltage behavior of $CH_3NH_3PbI_{3-x}Cl_x$ PSCs with three different electron-selective contacts (TiO_2, MgO-coated TiO_2, or Al_2O_3 scaffolds) over a wide range of light intensities under LS of I_0^{LS} = 1 sun. Changes in the photovoltage of PSCs from pristine to LS conditions based on a specific model that describes the charge distribution at the interface are explained. Evidence of photoinduced generation of an electrostatic potential (V_{elec}) and an increased recombination rate at the electron-selective contact−perovskite interface is confirmed. Thus, the contact−perovskite interface is "nonrigid" as it slowly builds up and changes during illumination and recovers even more slowly. The magnitude and effect of the V_{elec} and interfacial recombination on the photovoltage are very much dependent on the illumination intensity that generates the built-in potential (V_{bi}) and also on the I_0^{LS} duration. Although devices with both mp-TiO_2 and mp-Al_2O_3 scaffolds showed photoinduced changes, they were slightly less pronounced in PSCs with mp-Al_2O_3, probably due to the lower interfacial area with the semiconductive TiO_2 and the perovskite. The differences in the decay rate of V_{elec} between the LS stage and the dark recovery stage may reflect different ion migration processes in both stages. Under illumination (I_0^{LS}), generation of carriers across the perovskite drives ion drift (V_{elec} buildup) and ion drift is facilitated by electronic carrier screening, and in the dark, ions diffuse due to a concentration gradient (V_{elec} decay) and the overall conductivity decrease. We have also seen that a short 1 s light pulse can change the interfacial dynamics, meaning that ions can somewhat rearrange themselves at the interface in that time scale. As suggested previously, our results call for detailed reanalysis[31] of different types of measurements that require specific protocols to be developed in order to give reproducible and physically meaningful results of characterization techniques that use contacts.

EXPERIMENTAL METHODS

The materials and chemicals used in this study for device fabrication were purchased as follows: FTO glasses, TEC15 (Hartford Glass), titanium-tetraisopropoxide (Sigma-Aldrich), TiO_2 paste (18NRT, Dyesol), Al_2O_3 (Degussa AG), PbI_2, $PbCl_2$ (Sigma-Aldrich), DMSO (Fisher Scientific), 2-propanol (J.T. Baker), spiro-OMeTAD (Merck), chlorobenzene (Alfa Aesar), acetonitrile (J.T. Baker), bis(trifluoromethylsulfonyl)-imide lithium salt (Sigma-Aldrich), and 4-*tert*-butylpyridine (TBP, Sigma-Aldrich). The Al_2O_3 paste was prepared using a procedure described elsewhere.[23] TEC 15 fluorine-doped tin oxide-coated glass (dimensions: 71 × 71 mm^2) was used as the substrate for device fabrication. Each substrate was thoroughly cleaned with detergent, water, and ethanol before treatment with argon plasma for 4 min. The compact gradient TiO_2 blocking layer was deposited by a spray pyrolysis system in a procedure described elsewhere.[23] A precursor solution of 0.1 M titanium-tetraisopropoxide and acetyl acetone (1:1 ratio) in ethanol was sprayed on the preheated (450 °C) substrates, and the thickness of the blocking layer was calculated by using optical modeling. The mesoporous TiO_2 and Al_2O_3 scaffolds were 250−300 nm thick, deposited from diluted pastes (diluted with ethanol at a 1:10 ratio) on the TiO_2 blocking layer by spin-coating at 5000 rpm for 30 s. The substrates were then annealed at 550 °C for 90 min. The deposition of a thin layer of MgO onto TiO_2 was done exactly according to a protocol published elsewhere, as well as its comprehensive analysis and characterization.[23,32] A mixed lead halide solution was prepared using a 1 M/0.06 M ratio of $PbI_2/PbCl_2$ dissolved in DMSO and then stirred at 80 °C overnight. The synthesis of the methylammonium iodide (MAI) powder is described elsewhere.[33] A MAI solution (32 mg/mL in 2-propanol) was heated to 60 °C before use. The deposition of perovskite was performed by spin-coating $PbI_{2-x}Cl_x$ at 4000 rpm for 60 s on a mp-TiO_2 electrode, and the film was subsequently annealed at 100 °C for 60 min. Afterward, the films were dipped in the MAI solution for 2 min followed by washing with 2-propanol. Then, 50 μL of toluene was spun at 4000 rpm onto the perovskite film, which was exposed to MAI vapors for 60 min. The exposure was performed by holding the substrate upside down in a Pyrex glass box containing 200 mg of MAI powder heated at 140 °C. After vapor treatment, the substrates were annealed on a hot plate at 100 °C for 90 min. The hole transport material (HTM), spiro-OMeTAD, was dissolved in chlorobenzene (72 mg/mL) with the addition of 34 μL (540 mg/mL in acetonitrile) of bis(trifluoromethylsulfonyl)imide lithium salt (LiTFSI) and 58 μL (80 mM) of TBP. The HTM solution was spin-coated onto the perovskite films at 4000 rpm for 30 s. The substrates were kept in a drybox (air environment) overnight under dark conditions to dope the HTM with oxygen. A grid of 13 × 13 back contact silver electrodes (100 nm thick) was thermally evaporated on each substrate using a mechanical mask, forming a total of 169 devices (with a cell area of ∼0.026 cm2) fabricated on one substrate.

Device characterization: Current−voltage measurements were performed using a home-built automated scanning *iV* system described elsewhere[26] (note: during the *iV* scanning, each PSC in the library was illuminated individually without LS). Immediately after performing *iV* measurements, the devices were kept overnight in the dark in a nitrogen environment, prior to any LS measurement.

ASSOCIATED CONTENT

Supporting Information

The Supporting Information is available free of charge on the ACS Publications website at DOI: 10.1021/acsenergylett.7b00212.

Current−voltage (*i*−*V*) plot of a mp-TiO_2 PSC, dark recovery plots of photovoltage vs log I_0, and OCVD measurements (PDF)

AUTHOR INFORMATION

Corresponding Authors

*E-mail: bisquert@fca.uji.es (J.B.).
*E-mail: arie.zaban@biu.ac.il (A.Z.).

ORCID

Juan Bisquert: 0000-0003-4987-4887
Arie Zaban: 0000-0002-2315-6134

Author Contributions

§J.H and R.G have contributed equally to this work.

Notes

The authors declare no competing financial interest.

DOI: 10.1021/acsenergylett.7b00212
ACS Energy Lett. 2017, 2, 950−956

■ ACKNOWLEDGMENTS

The research of J.H. and L.G. received funding from the European Union Seventh Framework Program [FP7/2007-2013] under Grant Agreement 316494. We thank Hannah-Noa Barad, Adam Ginsburg, and David A. Keller for their assistance in substrate preparation and characterization. We acknowledge funding from MINECO of Spain under Project MAT2016-76892-C3-1-R and Generalitat Valenciana Project PROMETEOII/2014/020.

■ REFERENCES

(1) Chen, Q.; De Marco, N.; Yang, Y.; Song, T.-B.; Chen, C.-C.; Zhao, H.; Hong, Z.; Zhou, H.; Yang, Y. Under the Spotlight: The Organic−inorganic Hybrid Halide Perovskite for Optoelectronic Applications. *Nano Today* **2015**, *10*, 355−396.

(2) Zhao, C.; Chen, B.; Qiao, X.; Luan, L.; Lu, K.; Hu, B. Revealing Underlying Processes Involved in Light Soaking Effects and Hysteresis Phenomena in Perovskite Solar Cells. *Adv. Energy Mater.* **2015**, *5*, 1500279.

(3) Domanski, K.; Roose, B.; Matsui, T.; Saliba, M.; Turren-Cruz, S.-H.; Correa-Baena, J.-P.; Carmona, C. R.; Richardson, G.; Foster, J.; De Angelis, F.; et al. Migration of Cations Induces Reversible Performance Losses over Day/night Cycling in Perovskite Solar Cells. *Energy Environ. Sci.* **2017**, *10*, 604.

(4) Gottesman, R.; Zaban, A. Perovskites for Photovoltaics in the Spotlight: Photoinduced Physical Changes and Their Implications. *Acc. Chem. Res.* **2016**, *49*, 320−329.

(5) Delugas, P.; Caddeo, C.; Filippetti, A.; Mattoni, A. Thermally Activated Point Defect Diffusion in Methylammonium Lead Trihalide: Anisotropic and Ultrahigh Mobility of Iodine. *J. Phys. Chem. Lett.* **2016**, *7*, 2356−2361.

(6) Xiao, Z.; Yuan, Y.; Shao, Y.; Wang, Q.; Dong, Q.; Bi, C.; Sharma, P.; Gruverman, A.; Huang, J. Giant Switchable Photovoltaic Effect in Organometal Trihalide Perovskite Devices. *Nat. Mater.* **2014**, *14*, 193−198.

(7) Bae, S.; Kim, S.; Lee, S.-W.; Cho, K.; Park, S.; Lee, S.; Kang, Y.; Lee, H.-S.; Kim, D. Electric Field-Induced Degradation of Methylammonium Lead Iodide Perovskite Solar Cells. *J. Phys. Chem. Lett.* **2016**, *7*, 3091−3096.

(8) Yun, J. S.; Seidel, J.; Kim, J.; Soufiani, A. M.; Huang, S.; Lau, J.; Jeon, N. J.; Seok, S. I.; Green, M. A.; Ho-Baillie, A. Critical Role of Grain Boundaries for Ion Migration in Formamidinium and Methylammonium Lead Halide Perovskite Solar Cells. *Adv. Energy Mater.* **2016**, *6*, 1600330.

(9) Chen, S.; Wen, X.; Sheng, R.; Huang, S.; Deng, X.; Green, M. A.; Ho-Baillie, A. W.-Y. Mobile Ion Induced Slow Carrier Dynamics in Organic-Inorganic Perovskite $CH_3NH_3PbBr_3$. *ACS Appl. Mater. Interfaces* **2016**, *8*, 5351−5357.

(10) Li, C.; Tscheuschner, S.; Paulus, F.; Hopkinson, P. E.; Kießling, J.; et al. Iodine Migration and Its Effect on Hysteresis in Perovskite Solar Cells. *Adv. Mater.* **2016**, *28*, 2446−2454.

(11) Wu, Y.; Shen, H.; Walter, D.; Jacobs, D.; Duong, T.; Peng, J.; Jiang, L.; et al. On the Origin of Hysteresis in Perovskite Solar Cells. *Adv. Funct. Mater.* **2016**, *26*, 6807−6813.

(12) Bergmann, V. W.; Guo, Y.; Tanaka, H.; Hermes, I. M.; Li, D.; Klasen, A.; Bretschneider, S. A.; Nakamura, E.; Berger, R.; Weber, S. A. L. Local Time-Dependent Charging in a Perovskite Solar Cell. *ACS Appl. Mater. Interfaces* **2016**, *8*, 19402−19409.

(13) Zou, Y.; Holmes, R. J. Temperature-Dependent Bias Poling and Hysteresis in Planar Organo-Metal Halide Perovskite Photovoltaic Cells. *Adv. Energy Mater.* **2016**, *6*, 1501994.

(14) Wu, B.; Fu, K.; Yantara, N.; Xing, G.; Sun, S.; Sum, T. C.; Mathews, N. Charge Accumulation and Hysteresis in Perovskite-Based Solar Cells: An Electro-Optical Analysis. *Adv. Energy Mater.* **2015**, *5*, 1500829.

(15) Wojciechowski, K.; Stranks, S. D.; Abate, A.; Sadoughi, G.; Sadhanala, A.; Kopidakis, N.; Rumbles, G.; Li, C.-Z.; Friend, R. H.; Jen, A. K.-Y.; et al. Heterojunction Modification for Highly Efficient Organic-Inorganic Perovskite Solar Cells. *ACS Nano* **2014**, *8*, 12701−12709.

(16) Zarazua, I.; Bisquert, J.; Garcia-Belmonte, G. Light-Induced Space-Charge Accumulation Zone as Photovoltaic Mechanism in Perovskite Solar Cells. *J. Phys. Chem. Lett.* **2016**, *7*, 525−528.

(17) Gottesman, R.; Lopez-varo, P.; Gouda, L.; Jimenez-Tejada, J. A.; Hu, J.; Tirosh, S.; Zaban, A.; Bisquert, J. Dynamic Phenomena at Perovskite/Electron- Selective Contact Interface as Interpreted from Photovoltage Decays. *Chem.* **2016**, *1*, 776−789.

(18) Levine, I.; Nayak, P. K.; Wang, J. T. -W.; Sakai, N.; Van Reenen, S.; Brenner, T. M.; Mukhopadhyay, S.; Snaith, H. J.; Hodes, G.; Cahen, D. Interface-Dependent Ion Migration/Accumulation Controls Hysteresis in $MAPbI_3$ Solar Cells. *J. Phys. Chem. C* **2016**, *120*, 16399−16411.

(19) Zhang, H.; Liang, C.; Zhao, Y.; Sun, M.; Liu, H.; Liang, J.; Li, D.; Zhang, F.; He, Z. Dynamic Interface Charge Governing the Current-Voltage Hysteresis in Perovskite Solar Cells. *Phys. Chem. Chem. Phys.* **2015**, *17*, 9613−9618.

(20) Calado, P.; Telford, A. M.; Bryant, D.; Li, X.; Nelson, J.; O'Regan, B. C.; Barnes, P. R. F. Evidence for Ion Migration in Hybrid Perovskite Solar Cells with Minimal Hysteresis. *Nat. Commun.* **2016**, *7*, 13831.

(21) Kalanoor, B. S.; Gouda, L.; Gottesman, R.; Tirosh, S.; Haltzi, E.; Zaban, A.; Tischler, Y. R. Third-Order Optical Nonlinearity in Organometallic Methylammonium Lead Iodide Perovskite Films. *ACS Photonics* **2016**, *3*, 361−370.

(22) Gottesman, R.; Tirosh, S.; Barad, H.-N.; Zaban, A. Direct Imaging of the Recombination/Reduction Sites in Porous TiO_2 Electrodes. *J. Phys. Chem. Lett.* **2013**, *4*, 2822−2828.

(23) Gouda, L.; Boix, P. P.; Gottesman, R.; Ginsburg, A.; Keller, D. A.; Haltzi, E.; Hu, J.; Tirosh, S.; Anderson, A. Y.; Zaban, A. Open Circuit Potential Build-Up in Perovskite Solar Cells from Dark Conditions to 1 Sun. *J. Phys. Chem. Lett.* **2015**, *6*, 4640−4645.

(24) Tress, W.; Correa-Baena, J.; Saliba, M.; Abate, A.; Gratzel, M. Inverted Current−Voltage Hysteresis inMixed Perovskite Solar Cells: Polarization, Energy Barriers, and Defect Recombination. *Adv. Energy Mater.* **2016**, *6*, 1600396.

(25) Gouda, L.; Gottesman, R.; Tirosh, S.; Haltzi, E.; Hu, J.; Ginsburg, A.; Keller, D. A.; Bouhadana, Y.; Zaban, A. Vapor and Healing Treatment for $CH_3NH_3PbI_{3-x}Cl_x$ Films toward Large-Area Perovskite Solar Cells. *Nanoscale* **2016**, *8*, 6386−6392.

(26) Niemann, R. G.; Gouda, L.; Hu, J.; Tirosh, S.; Gottesman, R.; Cameron, P. J.; Zaban, A. Cs^+ Incorporation into $CH_3NH_3PbI_3$ Perovskite: Substitution Limit and Stability Enhancement. *J. Mater. Chem. A* **2016**, *4*, 17819−17827.

(27) Bertoluzzi, L.; Sanchez, R. S.; Liu, L.; Lee, J.-W.; Mas-Marza, E.; Han, H.; Park, N.-G.; Mora-Sero, I.; Bisquert, J. Cooperative Kinetics of Depolarization in $CH_3NH_3PbI_3$ Perovskite Solar Cells. *Energy Environ. Sci.* **2015**, *8*, 910−915.

(28) Gottesman, R.; Gouda, L.; Kalanoor, B. S.; Haltzi, E.; Tirosh, S.; Rosh-Hodesh, E.; Tischler, Y.; Quarti, C.; Mosconi, E.; De Angelis, F.; Zaban, A. Photoinduced Reversible Structural Transformations in Free-Standing $CH_3NH_3PbI_3$ Perovskite Films. *J. Phys. Chem. Lett.* **2015**, *6*, 2332−2338.

(29) Salvador, P.; Hidalgo, M. G.; Zaban, A.; Bisquert, J. Illumination Intensity Dependence of the Photovoltage in Nanostructured TiO_2 Dye-Sensitized Solar Cells. *J. Phys. Chem. B* **2005**, *109*, 15915−15926.

(30) Shao, S.; Abdu-Aguye, M.; Qiu, L.; Lai, L.-H.; Liu, J.; Adjokatse, S.; Jahani, F.; Kamminga, M. E.; ten Brink, G. H.; Palstra, T.; et al. Elimination of the Light Soaking Effect and Performance Enhancement in Perovskite Solar Cells Using a High Dielectric Constant Fullerene Derivative as Electron Extraction Material. *Energy Environ. Sci.* **2016**, *9*, 2444−2452.

(31) Nemnes, G. A.; Besleaga, C.; Tomulescu, A. G.; Pintilie, I.; Pintilie, L.; Torfason, K.; Manolescu, A. Dynamic Electrical Behavior of Halide Perovskite Based Solar Cells. *Sol. Energy Mater. Sol. Cells* **2017**, *159*, 197−203.

DOI: 10.1021/acsenergylett.7b00212
ACS Energy Lett. 2017, 2, 950−956

(32) Tachan, Z.; Hod, I.; Shalom, M.; Grinis, L.; Zaban, A. The Importance of the TiO_2/quantum Dots Interface in the Recombination Processes of Quantum Dot Sensitized Solar Cells. *Phys. Chem. Chem. Phys.* **2013**, *15*, 3841−3845.
(33) Gottesman, R.; Haltzi, E.; Gouda, L.; Tirosh, S.; Bouhadana, Y.; Mosconi, E.; De Angelis, F.; Zaban, A. Extremely Slow Photoconductivity Response of $CH_3NH_3PbI_3$ Perovskites Suggesting Structural Changes under Working Conditions. *J. Phys. Chem. Lett.* **2014**, *5*, 2662−2669.

DOI: 10.1021/acsenergylett.7b00212
ACS Energy Lett. 2017, 2, 950−956